Article

Integrated Taxonomy for *Halistemma* Species from the Northwest Pacific Ocean

Nayeon Park [1] , **Andrey A. Prudkovsky** [2,*] **and Wonchoel Lee** [1,*]

1   Department of Life Science, Hanyang University, Seoul 04763, Korea; skdus8974@naver.com
2   Faculty of Biology, Lomonosov Moscow State University, 119991 Moscow, Russia
*   Correspondence: aprudkovsky@wsbs-msu.ru (A.A.P.); wlee@hanyang.ac.kr (W.L.)

check for updates

Abstract: During a survey of the siphonophore community in the Kuroshio Extension, Northwest Pacific Ocean, a new *Halistemma* Huxley, 1859 was described using integrated molecular and morphological approaches. The *Halistemma isabu* sp. nov. nectophore is most closely related morphologically to *H. striata* Totton, 1965 and *H. maculatum* Pugh and Baxter, 2014. These species can be differentiated by their nectosac shape, thrust block size, ectodermal cell patches and ridge patterns. The new species' bracts are divided into two distinct types according to the number of teeth. Type A bracts are more closely related to ventral bracts in *H. foliacea* (Quoy and Gaimard, 1833) while Type B bracts are more similar to *H. rubrum* (Vogt, 1852). Each type differs, however, from the proximal end shape, distal process and bracteal canal. Both of the new species' morphological type and phylogenetic position within the genus *Halistemma* are supported by phylogenetic analysis of concatenated DNA dataset (mtCOI, 16S rRNA and 18S rRNA). Integrated morphological and molecular approaches to the taxonomy of siphonophores showed a clear delimitation of the new species from the congeners. *Halistemma isabu* sp. nov. is distributed with the congeners *H. rubrum*, *H. cupulifera*, *H. foliacea* and *H. striata* in the northwestern Pacific Ocean.

Keywords: zooplankton; jellyfish; mitochondria; systematics; hydrozoa

1. Introduction

Siphonophores, belonging to the class Hydrozoa Owen, 1843, live in oceans and are mostly holoplanktonic organisms [1]. Approximately, 190 species have been described as siphonophores, though there are likely more in the marine environment [2]. Siphonophores have gelatinous bodies and form unique colonies throughout their life [3]. Each individual in a colony has a variety of functions and morphological characteristics [4]. Siphonophorae are traditionally classified into three suborders (Calycophorae Leuckart, 1854; Cystonectae Haeckel, 1887; Physonectae Haeckel, 1888) depending on the presence of a gas bubble float, called a pneumatophore, and medusoids, known as nectophores [1,5,6]. Approximately 65 species with pneumatophores and nectophores are recognized as Physonectae [7]. Physonects's descriptions are often incomplete because Siphonophores have fragile gelatinous bodies and many research records are based on dissociated specimens, where only a few nectophores or bracts were collected [1,8]. Morphological changes throughout their life cycle, phenotypic plasticity and cryptic species are also responsible for erroneous species diversity estimations. Molecular methods can be used for species identification, reconstructing life cycles, and clarifying phylogeny [2,8–13].

Molecular data show that Cystonectae and Calycophorae are monophyletic taxa while Physonectae is polyphyletic [2,8]. Some families, such as Apolemiidae Huxley, 1859 and Pyrostephidae Moser, 1925, are not included in the clade unifying physonects and Calycophorae. Most physonects, however, can be combined into the monophyletic clade Euphysonectae. This includes Agalmatidae, Physophoridae

Eschscholtz, 1829, Forskaliidae Haeckel, 1888 and other families [2]. General Physonectae systematics and phylogenetic affinities of some genera are under debate.

Agalmatidae is the most specious family within the Physonectae. The family's diversity is limited to five genera (Agalmatidae *sensu stricto*) including short-stem (*Athorybia* Eschscholtz, 1829 and *Melophysa* Haeckel, 1888) and long-stem (*Agalma* Eschscholtz, 1825, *Halistemma* Huxley, 1859, *Nanomia* A. Agassiz, 1865) genera [6,7,14]. The short-stem genus *Athorybia*, with no nectophores, was previously classified outside of the Agalmatidae. However, molecular data show they are likely neotenic relatives of the *Agalma* species [2,8,14]. *Melophysa melo* (Quoy and Gaimard, 1827) has a spiral siphosome and tricornuate tentilla and is related to *Athorybia* and *Agalma* species [14]. Long-stem agalmatids (*Agalma*, *Halistemma*, *Nanomia*) include monoecious species with dorsal nectosoma and a descending mantle canal in its nectophores [6,7,14]. The agalmatid genera are delimited based on the nectophores' shape, ridge pattern, and tentilla type. Nevertheless, these morphologic differences and taxonomic boundaries were only generalized in a short Mapstone (2015) [7] review. *Halistemma*, which we address in this paper, is a genus established by Huxley (1859) [15]. It has a long taxonomic history which Pugh and Baxter (2014) [16] recently reviewed. A total of six *Halistemma* species are known.

In this study, we describe a new *Halistemma* species found in the Northwest Pacific Ocean. Our description uses morphological characteristics and a three-gene molecular approach.

2. Materials and Methods

2.1. Sample Collections

Plankton samples were collected in October 2019 during a R/V ISABU cruise in the Kuroshio Extension (Figure 1). We used a Multiple Opening/Closing Net and Environmental Sensing System (MOCNESS, 1×1 m^2, mesh size: 200 µm) towed between 200 m and the surface. Immediately after towing, we split plankton samples into 1/2 aliquots using a Folsom plankton splitter. For morphological observation, one aliquot was fixed in neutralized 5% formalin solution and stored at room temperature. For future molecular analysis, we fixed the other aliquot in 99.9% ethanol and stored at 4 °C. All material was deposited at the National Institute of Biological Resources (NIBR), Korea's invertebrate collection.
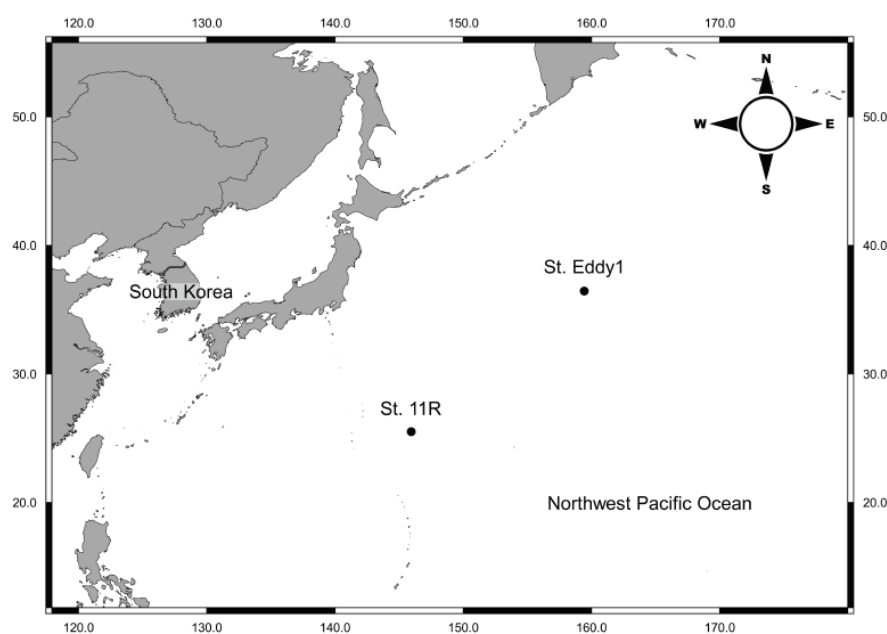

Figure 1. Map of sampling stations. (QGIS, Version: 3.6.0).

2.2. Morphological Analysis

For morphological observation, specimens were sorted from 5% neutralized formalin plankton samples using a Live Insect Forceps (26029-10, Fine Science Tools Inc., Foster City, CA, USA) and a stereomicroscope (Olympus SZX7, Tokyo, Japan). We placed sorted specimens in 20 mL glass vials with the formalin solution at room temperature. We observed specimens on a Petri dish (Ø: 5 cm) filled with 5% neutralized formalin solution under the stereomicroscope. We identified all specimens using descriptions and illustrations from Kirkpatrick and Pugh (1984) [17], Mapstone (2009) [18], Totton (1954) [19], Totton and Bargmann (1965) [1] and Pugh and Baxter (2014) [16] and used Pugh and Baxter (2014) [16] terminology. Digital photographs of specimens were taken using a digital camera (Olympus PEN Lite E-PL3, Tokyo, Japan) connected to the stereomicroscope with side lights on the dark field. We took the digital photographs at various focal points and performed multi-focus stacking using Helicon Focus 7 software (Version: 7.5.1). We cropped the photographed objects and moved them to a black background using the Levels tool in Adobe Photoshop CS6 software (Version: 13.0). Measurements were taken using AxioVision Imaging System 4.8 software (Version: 4.8.1.0) and illustrations were drawn using a drawing tube on the stereomicroscope.

2.3. DNA Extraction, Amplification and Sequencing

For molecular analysis, specimens were sorted from 99.9% ethanol plankton samples using a Live Insect Forceps and a stereomicroscope. Before DNA extraction, we separated each specimen and transferred them to distilled water for 12 h to wash and remove the ethanol. LaboPass™ Genomic Isolation-Tissue miniprep kit (Cosmogenetech Co., Seoul, Korea) was used to extract genomic DNA following the manufacturer's protocols. We amplified three genetic markers, mitochondrial cytochrome c oxidase subunit I (mtCOI), 16S ribosomal RNA (16S rRNA) and 18S ribosomal RNA (18S rRNA), via polymerase chain reaction (PCR) using the AccuPower® PCR PreMix (Bioneer Co., Daejeon, Korea), and performed thermal cycling using a TaKaRa Thermal Cycler Dice Touch TP350 (Takara Bio Inc., Kusatsu, Japan). We added 5 μL premix, 15 μL distilled water, 3 μL DNA template, and 1 μL each of the forward and reverse primers to achieve a 25 μL total reaction volume per tube. We used modified jgLCO1490 (5′-TGTAAAACGACGGCCAGTTNTCNACNAAYCAYAARGAYATTGG-3′) and modified jgHCO2198 (5′-CAGGAAACAGCTATGACTANACYTCNGGRTGNCCRAARAAYCA-3′) primers [20] for mtCOI (about 650–850 bp) gene amplification. The thermo-cycling conditions were an initial 5 min at 95 °C followed by 42 cycles of 20 secs at 95 °C, 1 min at 48 °C and 1 min at 72 °C, and ended with a final 5 min at 72 °C referenced and modified from Geller et al. (2013) [20]. We also used COF (5′-TGAGTATTTTCAACTAATCAYAAAGA-3′) and COR (5′-AAGTAAGCTCTAGTATCAACRTCCAT-3′) primers [21] for mtCOI. For this, the thermo-cycling conditions were 5 cycles of 50 sec 94 °C, 50 sec 45 °C, and 2 min 70 °C followed by 30 cycles of 50 sec 94 °C, 50 sec 50 °C, and 2 min 68 °C [21]. We used 16S-L (5′-GACTGTTTACCAAAAACATA-3′) and 16S-H (5′-CATAATTCAACATCGAGG-3′) primers [22] for 16S rRNA (about 600bp) gene amplification. The thermo-cycling conditions were 5 cycles of 1 min at 94 °C, 50 secs at 45 °C and 1 min at 72 °C followed by 30 cycles of 50 secs at 94 °C, 1 min at 50 °C and 1 min at 72 °C, and a final 5 min at 72 °C [23]. We used EukA (5′-AACCTGGTTGATCCTGCCAGT-3′) and EukB (5′-TGATCCTTCTGCAGGTTCACCTAC-3′) primers [24] for 18S rRNA (about 1800 bp) gene amplification. The thermo-cycling conditions were 30 cycles of 10 secs at 94 °C, 1 min at 38 °C and 3 min at 72 °C and a final 2 min at 94 °C [25]. To confirm the PCR product amplifications, we used electrophoresis on a 1% agarose gel (AGAROSE I™, Amresco Inc., Solon, USA; LaboPass™ Buffer 50X TAE, Cosmogenetech Co., Seoul, Korea) with Staining STAR (Dynebio Inc., Seongnam, Korea) for 20 min at 100V with a 100 bp DNA ladder (Bioneer Co., Daejeon, Korea). PCR products were purified for sequencing reactions using a LaboPass™ PCR Purification Kit (Cosmogenetech Co., Seoul, Korea) following the manufacturer's protocols. Purified PCR products were sent to Macrogen Inc. (Seoul, Korea) for DNA sequencing. Sequencing reactions using a DNA Engine Tetrad 2 Peltier Thermal Cycler (Bio-Rad laboratories Inc., Hercules, CA, USA) and an ABI Big Dye® Terminator v3.1 Cycle Sequencing Kit (Applied Biosystems, Waltham, MA, USA) following the

manufacturer's protocols. We performed single-pass sequencing on each template using the same primer set. Using Applied Biosystem's method, we purified the fluorescent-labeled fragments to remove unincorporated terminators and dNTPs and injected the electrophoresis samples into an ABI 3730xl DNA Analyzer (Applied Biosystems, Waltham, MA, USA). Due to its long length, the 18S rRNA additionally used the internal primer [26] for sequencing.

2.4. Species Delimitation and Phylogenetic Analysis

Finch TV software (Version: 1.4.0) read and cut sequences with low-quality signals, and once inspected, ClustalW [27] aligned forward and reverse sequences using default parameters embedded in Molecular Evolutionary Genetics Analysis 7 software (MEGA7, Version: 7.0.26). BLAST [28] analyses of the GenBank database were used to check that the sequences were Siphonophorae in origin and not contaminants. We acquired the mtCOI, 16S rRNA and 18S rRNA *Halistemma* sequences and other Siphonophorae sequences and used GenBank for the analysis. We constructed molecular analysis of the newly acquired sequences and the 142 Agalmatidae sequences (mtCOI: 37 and 16S rRNA: 19) and Siphonophorae (18S rRNA: 86) downloaded from GenBank (Table S1). The outgroup *Physalia physalis* (Linnaeus, 1758) was selected as belonging to Cystonectae (mtCOI and 16S rRNA) and the outgroup *Neoturris breviconis* (Murbach and Shearer, 1902) belonging to order Anthoathecata Cornelius, 1992 (18S rRNA). We calculated the genetic distances between alignment sequences using the Kimura 2-parameter (K2P) model [29] with complete deletion by MEGA7 software [30]. For *Halistemma*, we calculated the K2P genetic distances between the sequences and each of the three markers (mtCOI: 9, 16S rRNA: 10 and 18S rRNA: 6) (Tables S2–S4). In addition, we calculated K2P genetic distances for intraspecies, interspecies, intragenus and intergenus based on each of the three markers (mtCOI: 36, 16S rRNA: 19 and 18S rRNA: 13) within the Agalmatidae *sensu stricto* (Table S5). Maximum Likelihood (ML) and Bayesian Inference (BI) trees were drawn for phylogenetic analyses. The three single-gene ML phylogenetic trees' datasets included agalmatid sequences (mtCOI: 47, 16S rRNA: 26) and Siphonophorae (18S rRNA: 90). The concatenated BI and ML trees' datasets used 12 sequences from three concatenated Agalmatidae markers (mtCOI, 16S rRNA and 18S rRNA). To find the best-fit evolutionary model for the ML and BI analysis, we ran a Model Selection program using the MEGA7 software [30] and jModelTest software (Version: 2.1.7) [31,32] with the Akaike information criterion (AIC) [33–35]. Before creating the Nexus file, a FastGap (Version: 1.2) [36,37] was used to calibrate the Gap after alignment. The ML method used the best fit model proposed by Akaike information criterion with nearest neighbor interchange. This generated 1000 bootstrapping replicates for the phylogenetic tree reconstruction [38]. A BI tree was constructed using MrBayes software (Version: 3.2.6) [39–41] following likelihood parameters nst = 6 and rates = invgamma. We ran a Markov Chain Monte Carlo (MCMC) using the following parameters: ngen = 1,000,000, nchains = 4, samplefreq = 100, savebrlens = yes and printfreq = 1000. The BI trees were constructed using the "sump" command with burin = 250 to summarize parameters and the "sumt" command with burin = 250 to summarize the tree.

3. Results

3.1. Systematics

Phylum Cnidaria Hatschek, 1888
Class Hydrozoa Owen, 1843
Subclass Hydroidolina Collins, 2000
Order Siphonophorae Eschscholtz, 1829
Suborder Physonectae Haeckel, 1888
Family Agalmatidae Brandt, 1834
Genus *Halistemma* Huxley, 1859
Halistemma isabu sp. nov.

3.1.1. Etymology

The name "isabu" is derived from the R/V ISABU, the cruise on which the new species was discovered.

3.1.2. Locality

Type locality: Kuroshio extension, Northwest Pacific Ocean, (25°29.94′ N, 145°55.94′ E), depth 200 m; Additional locality: Kuroshio extension, Northwest Pacific Ocean, (36°26.68′ N, 159°25.65′ E), depth 200 m.

3.1.3. Material Examined

Holotype: One nectophore (NIBRIV0000876389). Paratype: Three nectophores, 17 bracts (NIBRIV0000876390–NIBRIV0000876395) collected by Nayeon Park. All specimens deposited at the National Institute of Biological Resources (Korea).

3.1.4. Measurements

See Table 1 for detailed measurements.

3.1.5. Nectophore Descriptions

Figures 2 and 3. The nectophore is an inverted bell-shape with axial wings and thrust block (Figure 2a,b). The axial wings have a petal-shape that ends sharply proximal outwards (Figure 2(a_1)). The sides of the nectophore are thick. The thrust block is high, big, thick and well-developed, rising above the axial wings (Figure 2(b_1)). Basic ridge pattern includes lateral, vertical lateral, upper lateral and lower lateral ridges. Upper lateral ridges (Figure 2(c_1)) make a hook-shaped curve in the proximal part and down the slope to the medial line of the nectophore (Figure 2c). There are many folds along the curve (Figure 2(c_2)). Both upper lateral ridges approach one another, forming a Y-shape (Figure 2(d_1)). In the proximal part of nectophore, before the Y-shape, there are many slanted folds facing to the center. These ridges continue pronounced in the nectophore's distal part towards the ostium level (Figure 2(a_2)). They then curve out as slightly raised lines and become parallel to the upper margin of the ostium before petering out on the surface of the nectophore. The upper lateral ridge pairs are incomplete at both distal ends. The lateral ridges form a distinct line overhanging the nectophore's surface (Figure 2(d_2)). The lateral ridges extend from near the ostium to the upper lateral ridges on both sides. Ostium regions of lateral ridges are located at the same level as the distal ends of upper lateral ridges. The proximal end of lateral ridges is split into three branches near the upper laterals, two of which are complete, and one is deficiently bent in a central direction (Figure 2(c_3)). There are incomplete oblique ridges between the upper lateral ridges and the lateral ridges (Figure 2(d_3)). There are long oval planes from the proximal apex of incomplete oblique ridges to the intersection point of Y-shape. The complete vertical lateral ridges run obliquely down from the upper lateral ridge to join with the lower lateral ridges. There are a pair of ectodermal cell patches on the triangular facet on each side between the upper and lower lateral and vertical lateral ridges of the nectophore. Some or all of these patches were destroyed on most nectophores. The lower lateral ridges pass along the lower lateral border of the nectophore. In the proximal part, the lower lateral ridges meet the upper lateral ridges in the axial wing. In the distal part of nectophore, the lower terminate distally on the lower lateral borders of the ostium (Figure 2(b_2)). The ostial regions are wider than the width of the mouth plate. The mouth plate is deeply divided, forming two round plates that overlap extensively in the mid-line. There are two stairs in nectosac towards the ostium (Figure 2(b_3)). The nectosac surface has a scale pattern. The mantle canal starts at the internal pedicular canal's proximal end, the ascending branch of the mantle canal goes to the proximal direction to the trust block center (Figure 2(e_1)). The descending branch of the mantle canal goes in a distal direction toward the lower side before the nectosac level (Figure 2(e_2)). The ascending branch is about 2/3 of the total

mantle canal. The descending branch of the mantle canal has a club at the proximal end. The pedicular canal arises from the mantle canals' intersection and goes down toward the central apex of the nectosac (Figure 2(e_3)). The stem attachment point is located in the proximal end of the internal pedicular canal (Figure 2(e_4)). The external pedicular canal was not preserved in the present material. At the central apex of the nectosac, four radial canals originate from the distal end of the internal pedicular canal, extend along the lateral surfaces of the nectosac. The upper canal passes straight down to the ostium level following the upper surface of the nectosac. The lower canal passes straight down to the ostium, descending vertically along the center of the nectophore's lower side. The lower canal has distal diverticula that go down to a point near the mouth plate and end in a club-shaped swelling. Lateral radial canals on the left and right sides are looped to the nectosac (Figure 2(a_3)).
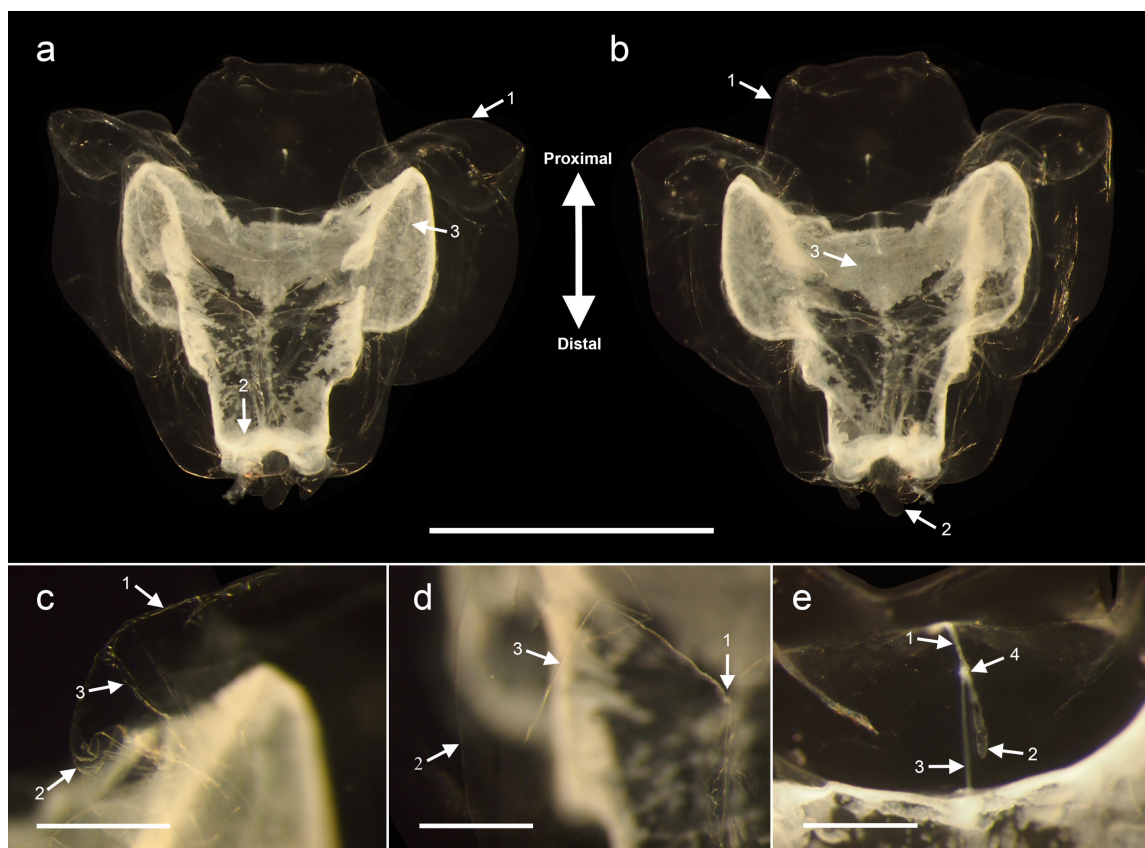

Figure 2. Digital images of *Halistemma isabu* sp. nov. (Nectophore). (**a**) Upper view; 1: Axial wings; 2: Ostium; 3: Lateral radial canal; (**b**) Lower view; 1: Thrust block; 2: Mouth plate; 3: Nectosac; (**c**) 1: Upper lateral ridges; 2: Hook shape of the upper lateral ridges; 3: Branched end of lateral ridges; (**d**) 1: Y-shape of the upper lateral ridges; 2: Lateral ridges; 3: Incomplete oblique ridges between the upper lateral ridges and the lateral ridges; (**e**) 1: Ascending branch of the mantle canal; 2: Descending branch of the mantle canal; 3: Internal pedicular canal, 4: Stem attachment point; Scale bar: (**a**,**b**) 5 mm; (**c**–**e**) 1 mm.

Table 1. *Halistemma isabu* sp. nov. Size measurement. N: Number of specimens, TL: Total Length (Proximal-Distal), TW: Total Width (Left-Right), OW: Ostium Width, NH: Nectosac Height (Proximal-Distal), NW: Nectosac Width (Left-Right), LAWW: Left Axial-wing Width, LAWH: Left Axial-wing Height, RAWW: Right Axial-wing Width, RAWH: Right Axial-wing Height, TBW: Thrust block Width, TBH: Thrust block Height, LMW: Left Mouth plate Width, LMH: Left Mouth plate Height, RMW: Right Mouth plate Width, RMH: Right Mouth plate Height, BALL: Bracteal attachment lamella Length, BCL: Bracteal canal Length.

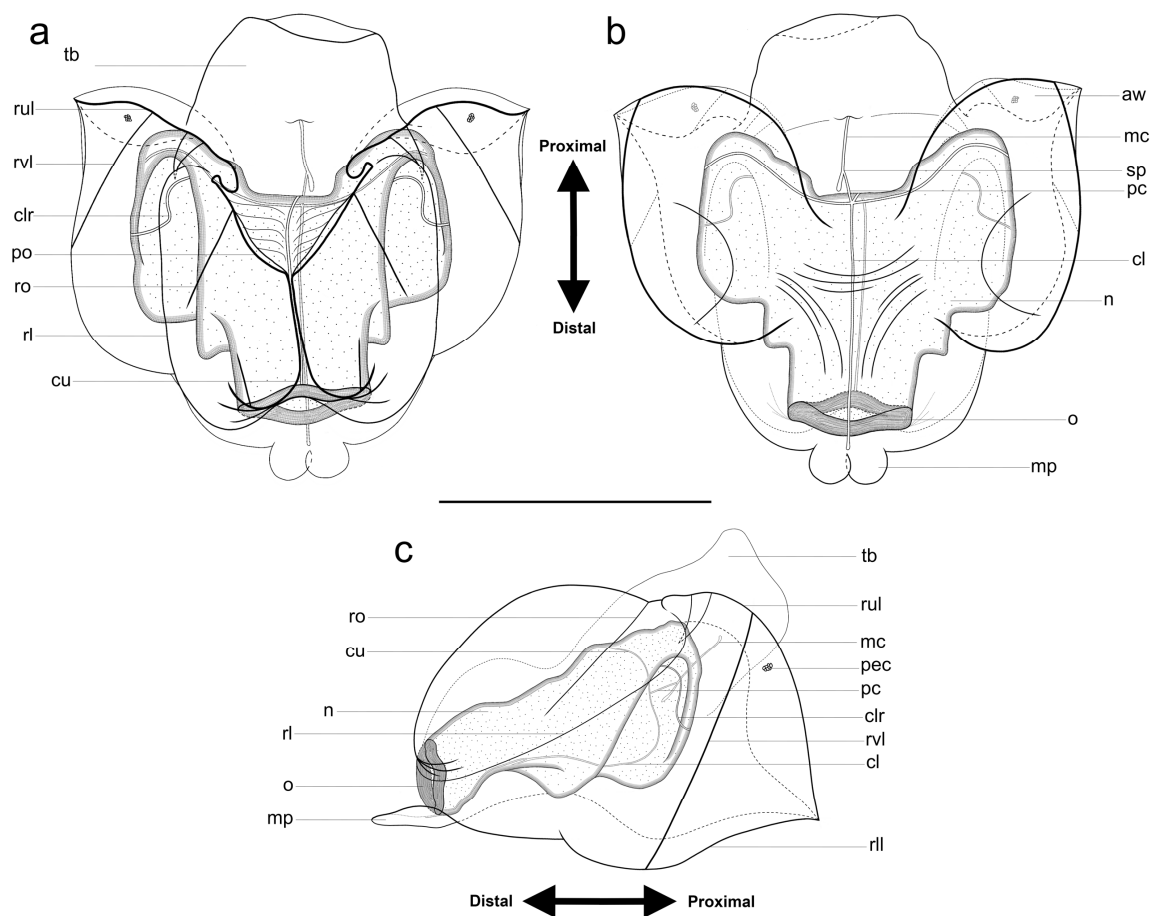| Specimens	Average (Min–Max) (mm)															
	N	TL	TW	OW	NSH	NSW	LAWW	LAWH	RAWW	RAWH	TBW	TBH	LMW	LMH	RMW	RMH
Nectophores	4	8.91 (7.99–9.87)	9.27 (8.27–10.86)	2.24 (1.57–2.73)	6.23 (5.48–7.05)	6.67 (5.64–7.45)	2.77 (2.44–2.93)	1.50 (0.74–1.80)	2.93 (2.69–3.04)	1.61 (0.95–2.01)	3.90 (3.16–4.91)	1.71 (1.54–1.97)	0.65 (0.48–0.79)	0.64 (0.49–0.84)	0.70 (0.46–0.85)	0.71 (0.59–0.82)
	N	TL	TW	BALL	BCL											
Bracts	17	15.39 (7.42–19.27)	5.72 (3.64–8.14)	5.22 (2.78–9.85)	1.36 (0.49–3.33)											

Figure 3. Illustration of *Halistemma isabu* sp. nov. (Nectophore). (**a**) Upper; (**b**) Lower; (**c**) Lateral views. tb: thrust block, aw: axial wing, pec: ectodermal cell patch, rul: upper lateral ridges, rvl: vertical lateral ridges, rl: lateral ridges, rll: lower lateral ridges, ro: obliquely ridges, po: oval plane, n: nectosac, sp: stem attachment point, mc: mantle canal, pc: pedicular canal, clr: lateral canal, cl: lower canal, cu: upper canal, o: ostium, mp: mouth plate; Scale bar: 5 mm.

3.1.6. Bract Descriptions

Figures 4 and 5. Bracts are leaf-shape with a sharp proximal end and a round distal end. The proximal ends are thicker than the distal ends. Bracts are slightly curled in the lower direction. A number of uncertain and irregular wrinkles appear on the centerline. On the distal end, there are one or two lateral teeth and a distal process (Figure 4(a_1,2)). There are a pair of ectodermal cell patches in the middle of the bracts, whose size and position vary considerably. In many cases, these patches were damaged. The proximal part of the bracts has a concave neck and narrowed end. The bracteal canal is elongated in the longitudinal direction of bract (Figure 4(a_3)). The bracteal attachment lamella, about 2/3 length of the bract is attached on the lower surface along part of the mid-line below the bracteal canals (Figure 4(a_4)). The bracteal canal is clearer than the bracteal attachment lamella and becomes sharper as it goes to both ends. The bracteal attachment lamellas are often damaged.
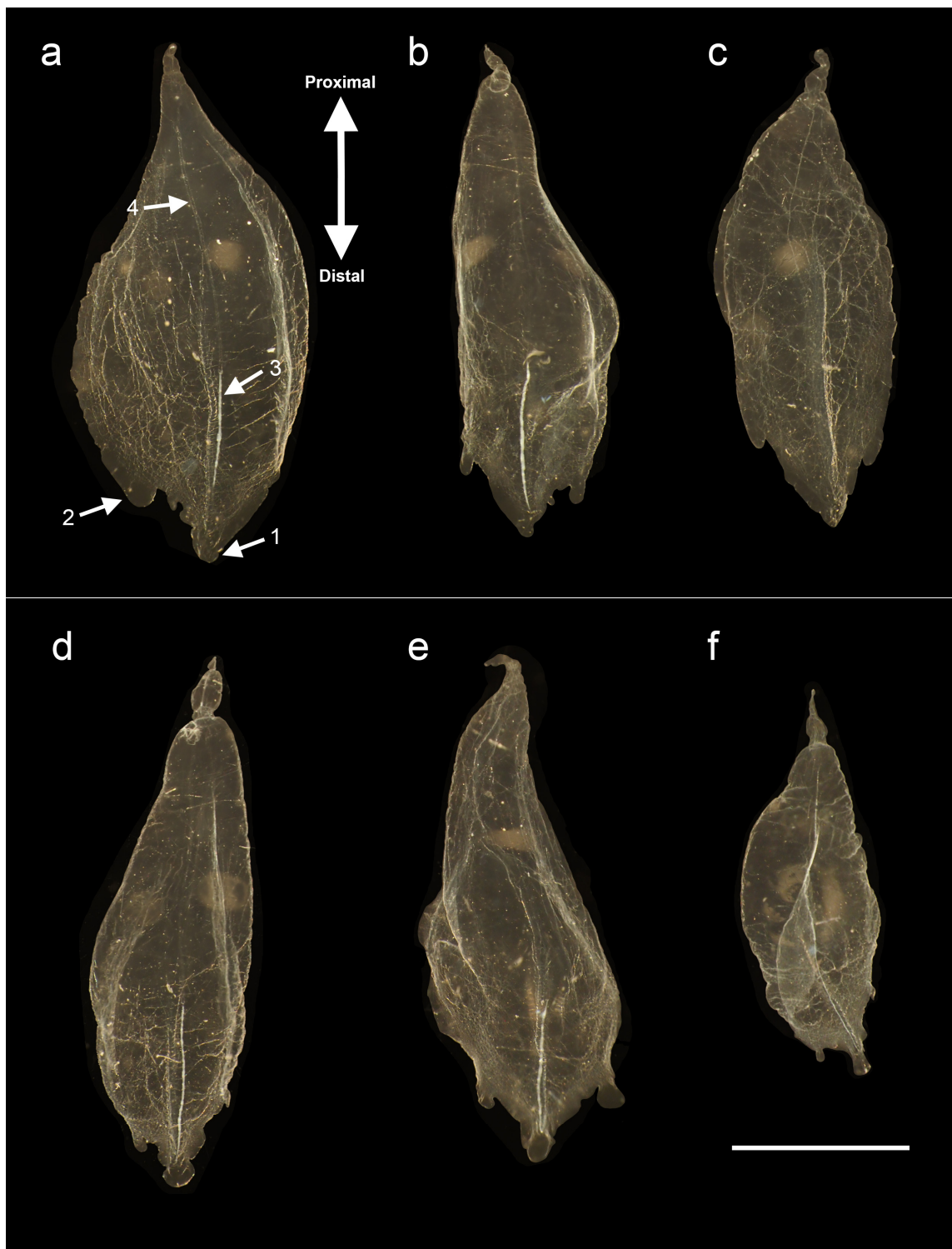
Figure 4. Digital images of *Halistemma isabu* sp. nov. (Bracts). (**a**) Type A_1 upper views: Distal process; 2: Lateral teeth; 3: Bracteal canal; 4: Bracteal attachment lamellas; (**b**–**f**) Type B upper views; Scale bar: 5 mm.
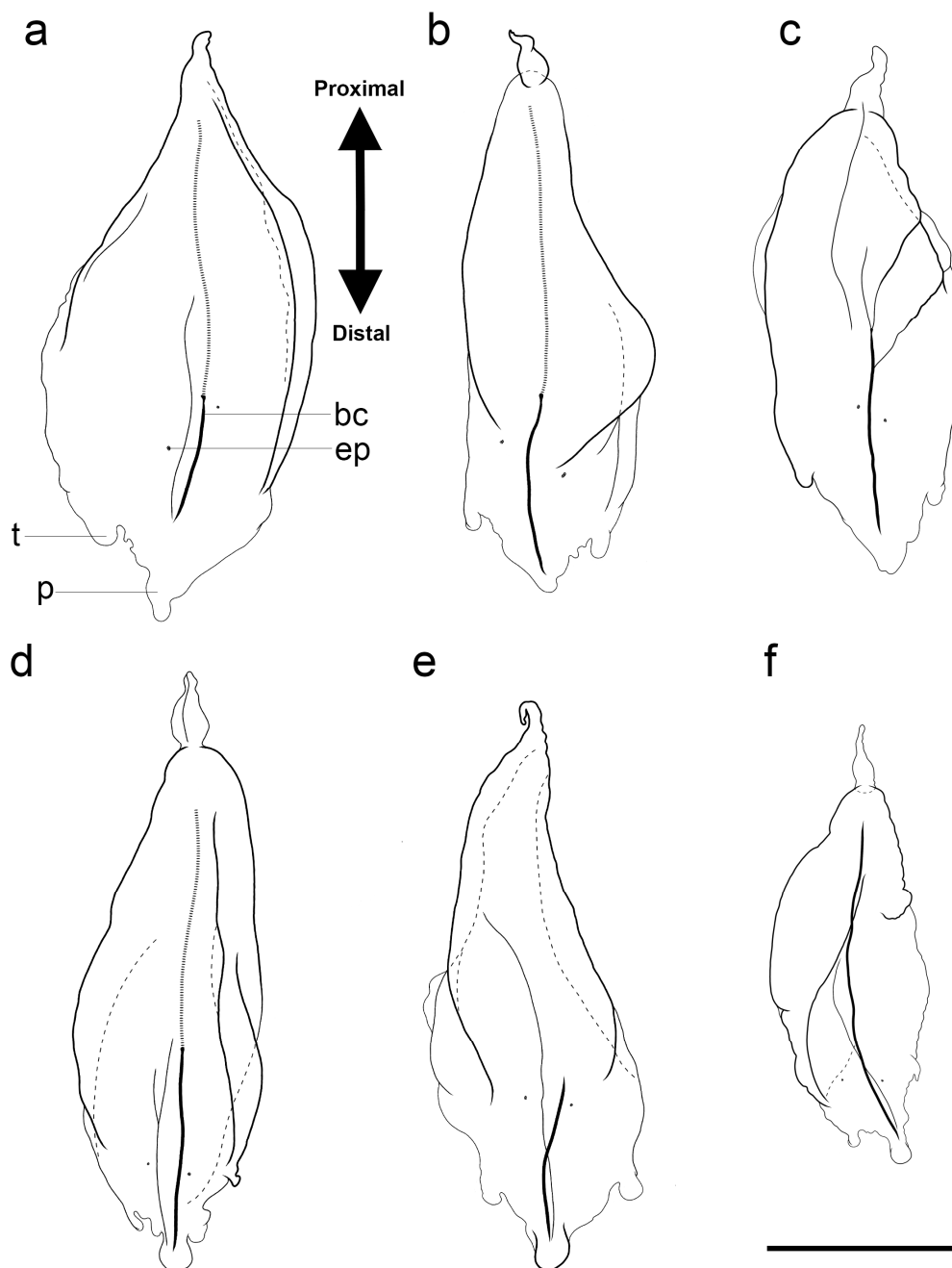
Figure 5. Illustration of *Halistemma isabu* sp. nov. (Bracts). (**a**) Type A upper views; (**b**–**f**) Type B upper views. bc: Bracteal canal, t: Lateral teeth, p: Distal process, ep: Ectodermal cell patches; Scale bar: 5 mm.

Although there are common features, bract shape is quite variable. There are ectodermal cell patches and lateral teeth for each specimen which we divided into two types (Type A: Figures 4a and 5a; Type B: Figures 4b–f and 5b–f). Type A has only one lateral tooth. It is broad and has a broad distally lateral indentation with an uneven outline near the distal process (Figure 5a). Type B has an elongated shape with a pair of lateral asymmetrical teeth in the distal part and distal process (Figure 5b,d–f). These bracts have two oblique furrows on the upper surface that run from the lateral sides of the bracts towards the middle line in the distal direction and form oblique flaps. A small pointed proximal process is separated by a constriction. One tooth is usually round and the other tooth more acute. The edge line between the tooth and the distal process sometimes has an uneven outline including bumps, cusps and small indentations (Figure 5b). Bract 5C lacked oblique furrows.

3.2. Molecular Phylogenetic Analysis

We obtained 15 new sequences of *Halistemma isabu* sp. nov.: six for mtCOI, six for 16S rRNA, and three for 18S rRNA (Table S1). We recovered the high-rank taxa phylogeny within Siphonophorae using a 18S rRNA-tree (Figure S1). Monophyletic Cystonectae (ML = 98) is a sister clade to Codonophora (the clade including all other siphonophores, ML = 99) and monophyletic Calycophorae (ML = 93) placed within the paraphyletic Physonectae. However, relationships between genera and species were obscured within the 18S rRNA-tree because of most nodes' low support values. Therefore, other genetic markers were used to analyze Agalmatidae *sensu stricto* phylogeny. Other single-gene trees (mtCOI and 16S rRNA, Figures S2 and S3) and the concatenated tree (Figure 6) produced congruent topologies; differences between trees are related to differences in taxon sampling. Node supports were lower in the single-gene trees while the concatenated dataset provided well-resolved and supported relationships. We recovered the genus *Halistemma* as monophyletic, but only two species were included in the concatenated dataset. *H. isabu* sp. nov. formed a clade with *H. rubrum* (Vogt, 1852) (PP = 0.95; ML = 88). Other unidentified *Halistemma* specimens from GenBank (GQ119989, GQ119991, KJ816934) were only included in either mtCOI or 16S rRNA datasets. They grouped with the *H. rubrum* and new species clade. Genus *Halistemma* was a sister clade to the group comprising *Agalma* and *Athorybia*. Genus *Agalma* was recovered as a paraphyletic group within the BI phylogenetic tree due to *Athorybia rosacea* (Forsskål, 1775) convergence with *Agalma okenii* Eschscholtz, 1825 (PP = 1). This paraphyly, however, was not supported within the ML phylogenetic tree. Finally, *Nanomia* was a sister taxon to the *Halistemma*, *Agalma* and *Athorybia* group.
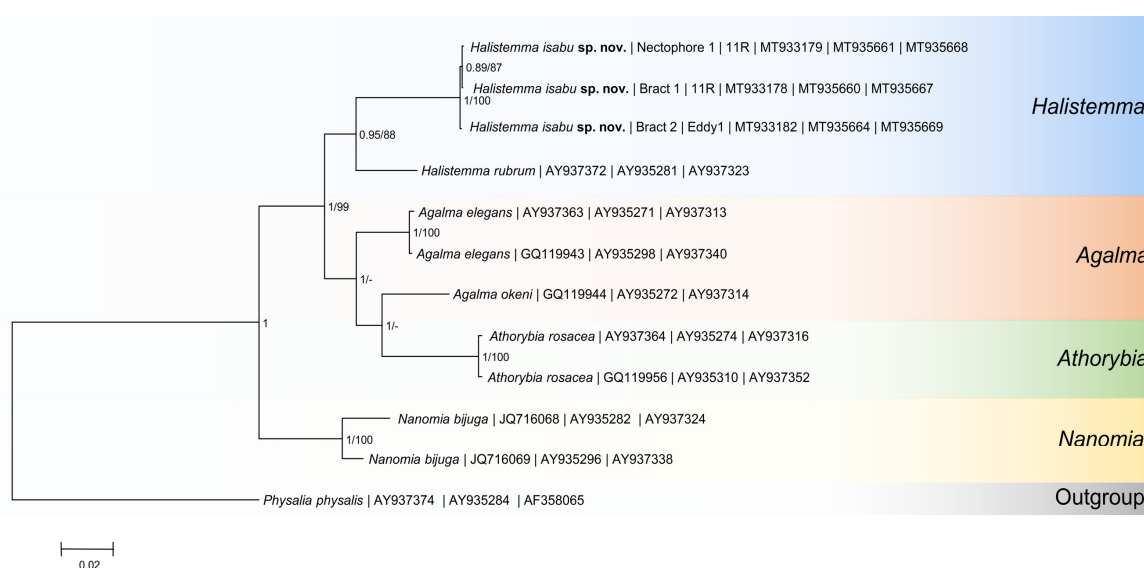

Figure 6. Molecular phylogenetic tree of family Agalmatidae based on concatenated data. Analysis involved 12 nucleotide sequences. All positions containing gaps and missing data were eliminated. The first number along the branches represents BI, the second number represents ML bootstrap values, and "-" indicates topologies not identical for BI and ML.

3.3. Agalmatidae Sensu Stricto Genetic Diversity

The K2P genetic distances between the new species' specimens ranged from 0 to 0.002 using the mtCOI dataset and from 0 to 0.011 using the 16S rRNA dataset (Tables S2 and S3). The K2P genetic distances between *Halistemma* species, including the new species, ranged from 0.118 to 0.124 in mtCOI and from 0.113 to 0.147 in 16S rRNA (Tables S2 and S3). Interspecies K2P genetic distances in mtCOI ranged from 0.138 to 0.150 for *Agalma* and from 0.168 to 0.172 for *Nanomia*. Interspecies K2P genetic distances in 16S rRNA ranged from 0.059 to 0.108 for *Agalma*. The intergenus divergence in mtCOI was minimal (0.134) between *Agalma-Halistemma* and maximal (0.212) between (*Halistemma-Nanomia*).

The intergenus divergence in 16S rRNA was minimal (0.083) between (*Agalma-Halistemma*) and maximal (0.510) between (*Agalma-Nanomia*).

4. Discussion

4.1. Agalmatid Family Phylogeny Based on Molecular Evidences

Dunn et al. (2005) [8] conducted a broad phylogenetic siphonophorans analysis using 18S-16S rRNA data; Munro et al. (2018) [2] used transcriptome data. They achieved well-supported results for the most nodes. Therefore, our main analysis purpose was to determine the new species *Halistemma isabu* sp. nov.'s phylogenetic position. Although six *Halistemma* species are known, only a few sequences are available in GenBank: *H. rubrum* sequences and two unidentified *Halistemma* specimens from unknown locations (GQ119989, KJ816934). *H. amphytridis* (Lesueur and Petit, 1807) was previously moved to the genus *Stephanomia* Lesueur and Petit, 1807 [16]. our molecular phylogenetic trees supported the genus *Halistemma* monophyly (Figure 6). The new species (*H. isabu* sp. nov.) grouped with *H. rubrum*, type species of the genus.

The K2P genetic distances between the new species showed low values. It is usually difficult to match species based on nectophore and bract morphology (unless the entire colony is collected). However, the low difference (0.000–0.002) shows that they are the same species. The larger K2P distances between specimen from GenBank (*H.* sp., *H.* sp. 1, *H. rubrum*) and collected specimen for the mtCOI gene (0.118–0.124) and for 16S rRNA (0.113–0.147) are more typically seen between species. Within Hydrozoans, Zheng et al. (2014) [23] showed the mean congeneric K2P distance based on mtCOI sequence data ranged from 0.045 to 0.243, while K2P distance based on 16S rRNA sequence data ranged from 0.062 to 0.236. The congeneric K2P distances among other long-stem agalmatid species (*Agalma*, *Halistemma*, *Nanomia*) ranged from 0.098 to 0.172 for the mtCOI gene and from 0.059 to 0.149 for the 16S rRNA gene. These estimates cannot be considered conclusive due to the lack of GenBank data. We can, however, consider the genetic divergences seen between *H. isabu* sp. nov., and other *Halistemma* species. These are similar to interspecific distances among other agalmatids.

Our results confirm previous phylogenies by Dunn et al. (2005) [8] and Munro et al. (2018) [2] with higher support values using the concatenated sequences and three markers. With the exception of the concatenated ML Agalmatidae tree, the three trees, mtCOI, 16S rRNA (ML), and concatenated (BI), had exactly the same topology (*Halistemma-Agalma-Athorybia* composed a big monophyletic clade). However, the concatenated BI tree shows *Agalma* as a paraphyletic group with a high support value (PP = 1). In contrast, the concatenated ML tree supports *Agalma* as a monophyletic group (ML = 77). This suggests that *Agalma* and *Athorybia*'s phylogenic position is unclear. Therefore, we excluded *Athorybia* from the genetic distances analysis. The single-gene tree also has limitations in revealing distinct topology. In order to get a clearer phylogenetic tree, we need to use additional markers while adding more data on the other *Halistemma* and Siphonophorae.

4.2. Morphological Comparisons of Halistemma Species

Pugh and Baxter (2014) [16] provided a diagnosis of the genus *Halistemma*. "Diagnosis: Agalmatid siphonophores with the characteristic arrangement of ridges on the nectophores; basically consisting of pairs of upper and lower lateral, lateral, and vertical lateral. Characteristic sinuous arrangement of the lateral radial canals on the nectosac. Adult bracts of at least two different types. In development, the colonies pass through a distinctive post-larval nectalia stage. Tentilla with single terminal filament, often ending in a cupulate process. Involucrum vestigial or covering only first one or two spirals of cnidoband."

Halistemma species are different mainly in nectophore, bract and tentilla morphology [16]. Since tentilla were absent in the specimen we collected, we focused our attention on nectophore and bract morphology. We compared the new species with other congeneric species based on Pugh and Baxter (2014) [16]'s description (Table 2).

Table 2. Morphological comparisons between the new species and other Halistemma species. O: presence, X: absence. * Type species.

Species	Size (Length × Width) (mm)	Upper Lateral Ridges Shape	Lateral Ridges	Vertical Lateral Ridges	Mouth Plate	Thrust Block Size	Nectosac Shape	Ridges between Upper Lateral and Lateral	Ascending Branch of Mantle Canal Length
H. isabu sp. nov.	~9.9 × 10.9	Obliquely inward (Y-shape with hook)	2 pairs complete, 1 pair incomplete	1 pair complete	O, deeply divided	>Axial wing	T-shape with stair	O, 1 pair incomplete	>descending branch
H. striata	~23 × 25	Obliquely inward (Y-shape with stair)	1 pair complete	3 pairs complete, 1 pair incomplete	O, deeply divided	≤Axial wing	T-shape	X	>descending branch
H. foliacea	~20 × 22	Obliquely inward (Obscure Y-shape)	1 pair incomplete	2 pairs complete	O, slightly emarginated	<Axial wing	T-shape	X	=descending branch
H. rubrum *	~7 × 7	Vertically straight	1 pair incomplete	1 pair incomplete	X	<Axial wing	T-shape	X	=descending branch
H. maculatum	~11 × 10	Obliquely inward (V-shape)	1 pair complete	1 pair complete	O, deeply divided	≥Axial wing	T-shape	X	=descending branch
H. cupulifera	~9.5 × 9	Obliquely inward (V-shape)	1 pair complete	1 pair complete	O, slightly emarginated	≥Axial wing	T-shape	X	=descending branch
H. transliratum	~13 × 13.4	Obliquely inward (V-shape)	1 pair complete	1 pair complete	X	<Axial wing	T-shape	X	>descending branch

Halistemma nectophores are different in vertical ridge number, ridge completeness, trust block size compared to axial wing size, and mouth plate presence. General nectophore shape varied from ovate-triangular in *H. rubrum* and *H. transliratum* Pugh and Youngbluth, 1988 to triangular with a step (T-shape) in *H. cupulifera* Lens and van Riemsdijk, 1908, *H. striata* Totton, 1965, *H. maculatum* Pugh and Baxter, 2014 and the new species. There are between one and several ectodermal cell patch pairs on *Halistemma*'s nectophore sides except in *H. foliacea* (Quoy and Gaimard, 1833) (one pair on *H. striata*; two pairs on *H. rubrum*, *H. cupulifera* and *H. maculatum*; several on *H. transliratum*). The new species has an ectodermal cell patch pair like *H. striata*. These patches, however, were often abraded in the collected specimen. The trust block's size to axial wing ratio is dissimilar in different *Halistemma* species. Some species, including *H. cupulifera* and *H. striata*, have a massive square trust block extending up to the axial wings' level. In the new species' nectophores, the trust block extends above the axial wings' level. The mouth plate is present in *H. cupulifera*, *H, striata*, *H. foliacea*, *H. maculatum*. It is almost undivided in *H. cupulifera* and *H. foliacea*, moderately divided in *H. striata* and deeply divided in *H. maculatum* and the new species. A pair of upper lateral ridges converge in the nectophore's distal part forming a V-shape in *H. cupulifera* and *H. maculatum* and a Y-shape in *H. striata* and the new species. This is an intermediate characteristic in *H. rubrum* and *H. foliacea* and variable in *H. transliratum*. Only two species, *H. foliacea* and *H. striata*, have about 20 mm and larger nectophores. Nectophore size correlates with the number of vertical lateral ridges on its surface. *H. foliacea* nectophores have two vertical lateral ridge pairs and *H. striata* nectophores have three vertical lateral ridge pairs. Nectophores of other species are smaller and have only one pair of vertical lateral ridges.

Different species' ridge completeness is also important. Vertical lateral ridges are incomplete in *H. rubrum* and do not join with lower laterals. The lateral ridges' proximal part is incomplete in *H. rubrum* and *H. foliacea*. The new species has three branches in the lateral ridges' proximal part, two of which are complete and one incomplete. The upper lateral ridges form two branches in the nectophore's distal part in H. *transliratum* and little branchlets near the ostium in *H. foliacea*. The nectosac is mainly T-shape in *Halistemma* species, but there is an additional step in the nectosac's proximal part in *H. striata*. In the new species, the nectosac's step is located in its distal part. The mantle canal includes ascending and descending branches in all *Halistemma* species. The ascending and descending branch lengths are about equal in *H. rubrum*, *H. foliacea*, *H. cupulifera* and *H. maculatum*. The mantle canal's ascending branch is slightly longer than the descending branch in *H. striata*, and the ascending branch is approximate twice the descending branch length in *H. transliratum* and the new species. The radial canals are typical for all species. The upper and lower canals are straight, and the lateral canals have a similar looped pattern. In *H. transliratum,* the lateral radial canals are often irregular and occasionally small diverticula branch off at various places along their length. All radial canals fall into the ostial ring canal. In the new species, however, small diverticulum issue from the lower canal and runs distally within mouth plate.

Characteristics may differ depending on the specimen's maturity. Pugh and Baxter (2014) [16] studied young *Halistemma* species' nectophores. The trust block's size to axial wing ratio changes during the nectophore maturation. In young nectophores, the central thrust block is usually very flat and undeveloped so that the relatively large axial wings extend well beyond. During maturation, the upper lateral ridges' proximal part and axial wings diverge to the nectophores sides leaving room for the protruding trust block. The very young nectophoral bud clearly shows the ridge pattern in *H. rubrum*. The ridge pattern is usually present in young nectophores and does not change during maturation. The lateral ostial processes are prominent in young nectophores (in *H. rubrum*, *H. foliacea*) but become relatively small in mature nectophores. The mouth plate became visible in *H. cupulifera*, *H, striata*, *H. foliacea*, *H. maculatum* mature nectophores. We assumed that our collected specimen's characteristics, such as prominent trust block, lateral ostial process absence, and Y-shaped upper lateral ridge pair, represent mature nectophores.

The new species has unique morphological features. Lateral ridge ends are split into three branches near the upper lateral ridges, two of which are complete and one which is deficiently bent in

a central direction. Before the upper lateral ridges go to the nectophore's median line, they go through a hook-shaped curve. An incomplete oblique ridge pair issues from below the upper lateral ridges' hook-shaped curve in the lateral ridge's direction.

We conclude that some of the new species' characteristics are similar to *H. striata* and *H. maculatum*. For example, the ridge pattern and mouth plate shape are similar to *H. maculatum* except for the lateral ridges' proximal part, which are divided to three branches with additional incomplete lateral ridges. The shape of nectosac, one pair of ectodermal patch and the upper lateral ridges' Y-shape brings it closer to *H. striata*. *Stephanomia rubra* "f" by Totton (1954) [19] from Indian Ocean has a step-shaped nectosac, a hook-shaped upper lateral ridge curve and a prominent trust block. All of these characteristics are similar to specimens examined in this study. Pugh and Baxter (2014) [16] described the similarities between Totton's specimen "f" with *H. maculatum*. However, *H. maculatum*'s nectosac is different from specimen "f" and *H. isabu* sp. nov. Totton's specimen has typical lateral ridge proximal ends as in *H. maculatum* while *H. isabu* sp. nov. nectophores have three lateral ridge proximal end branchelets.

Bracts are very variable and change during maturation. Larval bracts were studied in *H. rubrum*, *H. transliratum*, and *H. maculatum*'s nectalia-stage. These bracts are symmetrical and elongated with a prominent distal process. Otherwise, larval bract characteristics differ significantly from adult bract characteristics. There are two pairs of teeth in larval bracts of *H. rubrum* and *H. maculatum*. The proximal teeth pair is very close to the larval bract's proximal end. *H. rubrum* has two ectodermal cell patch pairs in their larval bracts compared to one pair in adult bracts. The *H. maculatum* ectodermal cell patches' number and position differed greatly between the larval and adult bracts. Larval bracts in *H. transliratum* are similar to adult bracts type "A" in their elongated shape, but the morphology is simplified in the larval type compared to the adult type. Species such as *H. striata* and *H. foliacea* has young bracts descriptions. Maturing and mature bract differences were not significant and predominantly concerned shape changes. We conclude that the new species' bracts are not similar to larval bracts because of their shape asymmetry, short distal process and complex morphology.

Bract classification does not yet have uniform principles. For example, bracts A and B in *H. rubrum* or A and C in *H. cupulifera* were classified based on their lateral teeth's shape and position. Shape is an important characteristic for *H. foliacea* bract classification, but bract classification for the rest of the species (*H. cupulifera*, *H. striata*, *H. transliratum*, *H. maculatum*) is based mainly on teeth number of ectodermal cell patch numbers. We found two bract types in *Halistemma isabu* sp. nov. Type A (Figures 4a and 5a) are similar to *H. foliacea*'s ventral bracts because they have distally broad lateral indentations. They differed however, from *H. foliacea*'s teeth pair, proximal end shape, and bracteal canal. Bracts B of *H. isabu* sp. nov. are similar to *H. rubrum*'s bracts A. In both species, the bracts have a narrowed proximal end with a concave neck, one teeth pair and one ectodermal cell patch pair. However, the new species' bracts B are more concave and have uneven distal end contours. Unlike *H. maculatum*'s bracts A, the new species' bracts B have a small distal process and only one ectodermal cell patch pair.

4.3. Geographic Distribution of Halistemma

The new species was collected in the Kuroshio Extension in the Pacific Ocean. It differs from the other species' type localities (*H. rubrum*: Mediterranean Sea; *H. cupulifera*: Banda Sea; *H. foliacea*: New Guinea; *H. maculatum and H. transliratum*: Bahamas, North Atlantic Ocean; *H. striata*: Bermuda). In subsequent records, most *Halistemma* (*H. rubrum, H. cupulifera, H. striata, H. transliratum, H. maculatum*) are found mainly in the Atlantic Ocean [42–45]. *H. rubrum*, *H. cupulifera*, *H. foliacea* and *H. striata* are also found in the North Pacific Ocean [9,46–48]. *H. rubrum*, *H. cupulifera*, *H. maculatum* are also found in other areas including the Indian Ocean and the Mediterranean Sea [1,49–51]. Based on these records, *H. rubrum* and *H. cupulifera* are considered cosmopolitan species. *H. striata*, *H. transliratum*, *H. maculatum* and *H. foliacea* show a limited distribution. The species most consistent with the new species' finding are *H. rubrum*, *H. cupulifera*, *H. foliacea* and *H. striata*. These are found in the north Pacific Ocean, particularly near Japan, in Sagami Bay, which is the closest region to the new species'

sampling sites. Most *Halistemma* species' wide geographical distribution and their coexistence in the same localities require a more accurate analysis and their phylogenetic position should be checked using molecular methods.

5. Conclusions

In this study, we conducted a morphological and molecular analysis of *H. isabu* sp. nov. found in the Kuroshio Extension of Northwest Pacific Ocean. We provided information about the new species including digital photographs, illustrations, measurements, and DNA sequencing (mtCOI, 16S rRNA and 18S rRNA). We compared the new species morphologically to *Halistemma* congeneric species, and using a molecular approach, confirmed that the new species formed a monophyletic clade with other *Halistemma* species. We also calculated Agalmatidae *sensu stricto* genetic distances. These data and discussions are an important contribution to the controversial Agalmatidae taxonomy research.

Supplementary Materials: The following are available online at http://www.mdpi.com/2073-4441/12/11/3283/s1, Table S1: Accession numbers of sequences used in this study's phylogenetic analyses, Table S2: K2P distances of mtCOI sequences between genus *Halistemma* from Genbank and this study, Table S3: K2P distances of 16S rRNA sequences between genus *Halistemma* from Genbank and this study, Table S4: K2P distances of 18S rRNA sequences between genus *Halistemma* from Genbank and this study, Table S5: Estimates of average K2P distances over sequence pairs within family Agalmatidae, based on mtCOI, 16S rRNA and 18S rRNA gene data, Figure S1: Molecular phylogenetic tree of family Agalmatidae based on 18S rRNA data using the maximum likelihood method, Figure S2: Molecular phylogenetic tree of family Agalmatidae based on mtCOI data using the maximum likelihood method, Figure S3: Molecular phylogenetic tree of family Agalmatidae based on 16S rRNA data using the maximum likelihood method.

Author Contributions: All authors contributed to the study conception and design. Sample and data collection, N.P. and W.L.; Data analysis, N.P. and A.A.P.; writing—original draft preparation, N.P.; writing—review and editing, A.A.P. and W.L. All authors have read and agreed to the published version of the manuscript.

Conflicts of Interest: The authors declare no conflict of interest. The funders had no role in the design of the study; in the collection, analyses, or interpretation of data; in the writing of the manuscript, or in the decision to publish the results.

References

1. Totton, A.K.; Bargmann, H.E. British Museum (Natural History). In *A Synopsis of the Siphonophora*; British Museum (Natural History): London, UK, 1965; 232p.
2. Munro, C.; Siebert, S.; Zapata, F.; Howison, M.; Damian-Serrano, A.; Church, S.H.; Goetz, F.E.; Pugh, P.R.; Haddock, S.H.; Dunn, C.W. Improved phylogenetic resolution within Siphonophora (Cnidaria) with implications for trait evolution. *Mol. Phylogenetics Evol.* **2018**, *127*, 823–833. [CrossRef] [PubMed]
3. Pugh, P. The vertical distribution of the siphonophores collected during the SOND cruise, 1965. *J. Mar. Biol. Assoc. United Kingd.* **1974**, *54*, 25–90. [CrossRef]
4. Dunn, C.W.; Wagner, G.P. The evolution of colony-level development in the Siphonophora (Cnidaria: Hydrozoa). *Dev. Genes Evol.* **2006**, *216*, 743–754. [CrossRef] [PubMed]
5. Pugh, P. Siphonophorae. In *South Atlantic zooplankton*; Boltovskoy, D., Ed.; Backhuys Publishers: Leiden, The Netherlands, 1999; pp. 467–512.
6. Mapstone, G.M. Global diversity and review of Siphonophorae (Cnidaria: Hydrozoa). *PLoS ONE* **2014**, *9*, e87737. [CrossRef] [PubMed]
7. Mapstone, G. Systematics of siphonophores. In *Evolution of Venomous Animals and Their Toxins*; Springer: Dordrecht, The Netherlands, 2015; pp. 319–366.
8. Dunn, C.W.; Pugh, P.R.; Haddock, S.H. Molecular phylogenetics of the Siphonophora (Cnidaria), with implications for the evolution of functional specialization. *Syst. Biol.* **2005**, *54*, 916–935. [CrossRef]

9.　Grossmann, M.M.; Lindsay, D.J. Diversity and distribution of the Siphonophora (Cnidaria) in Sagami Bay, Japan, and their association with tropical and subarctic water masses. *J. Oceanogr.* **2013**, *69*, 395–411. [CrossRef]

10.　Grossmann, M.M.; Lindsay, D.J.; Collins, A.G. The end of an enigmatic taxon: Eudoxia macra is the eudoxid stage of Lensia cossack (Siphonophora, Cnidaria). *Syst. Biodivers.* **2013**, *11*, 381–387. [CrossRef]

11.　Grossmann, M.M.; Collins, A.G.; Lindsay, D.J. Description of the eudoxid stages of Lensia havock and Lensia leloupi (Cnidaria: Siphonophora: Calycophorae), with a review of all known Lensia eudoxid bracts. *Syst. Biodivers.* **2014**, *12*, 163–180. [CrossRef]

12.　O'Hara, T.D.; Hugall, A.F.; MacIntosh, H.; Naughton, K.M.; Williams, A.; Moussalli, A. Dendrogramma is a siphonophore. *Curr. Biol.* **2016**, *26*, R457–R458. [CrossRef]

13.　Panasiuk, A.; Jażdżewska, A.; Słomska, A.; Irzycka, M.; Wawrzynek, J. Genetic identity of two physonect siphonophores from Southern Ocean waters–the enigmatic taxon Mica micula and Pyrostephos vanhoeffeni. *J. Mar. Biol. Assoc. United Kingd.* **2019**, *99*, 303–310. [CrossRef]

14.　Pugh, P. The taxonomic status of the genus Moseria (Siphonophora, Physonectae). *Zootaxa* **2006**, *1343*, 1–42. [CrossRef]

15.　Huxley, T.H. *The Oceanic Hydrozoa; A Description of the Calycophoridae and Physophoridae Observed during the Voyage of HMS "Rattlesnake" in the Years 1846-50*; Royal Society: London, UK, 1859.

16.　Pugh, P.; Baxter, E. A review of the physonect siphonophore genera Halistemma (Family Agalmatidae) and Stephanomia (Family Stephanomiidae). *Zootaxa* **2014**, *3897*, 1–111. [CrossRef] [PubMed]

17.　Kirkpatrick, P.; Pugh, P. *Siphonophores and Velellids: Keys and Notes for the Identification of the Species*; Brill Archive: Leiden, The Netherlands, 1984; Volume 29.

18.　Mapstone, G.M. *Siphonophora (Cnidaria, Hydrozoa) of Canadian Pacific Waters*; NRC Research Press: Ottawa, ON, Canada, 2009.

19.　Totton, A.K. Siphonophora of the Indian Ocean together with systematic and biological notes on related specimens from other oceans. *Disc Rep.* **1954**, *27*, 1–162.

20.　Geller, J.; Meyer, C.; Parker, M.; Hawk, H. Redesign of PCR primers for mitochondrial cytochrome c oxidase subunit I for marine invertebrates and application in all-taxa biotic surveys. *Mol. Ecol. Resour.* **2013**, *13*, 851–861. [CrossRef]

21.　Schuchert, P. DNA barcoding of some Pandeidae species (Cnidaria, Hydrozoa, Anthoathecata). *Rev. Suisse De Zool.* **2018**, *125*, 101–127.

22.　Ender, A.; Schierwater, B. Placozoa are not derived cnidarians: Evidence from molecular morphology. *Mol. Biol. Evol.* **2003**, *20*, 130–134. [CrossRef]

23.　Zheng, L.; He, J.; Lin, Y.; Cao, W.; Zhang, W. 16S rRNA is a better choice than COI for DNA barcoding hydrozoans in the coastal waters of China. *Acta Oceanol. Sin.* **2014**, *33*, 55–76. [CrossRef]

24.　Medlin, L.; Elwood, H.J.; Stickel, S.; Sogin, M.L. The characterization of enzymatically amplified eukaryotic 16S-like rRNA-coding regions. *Gene* **1988**, *71*, 491–499. [CrossRef]

25.　Collins, A.G. Towards understanding the phylogenetic history of Hydrozoa: Hypothesis testing with 18S gene sequence data. *Sci. Mar.* **2000**, *64*, 5–22. [CrossRef]

26.　Strychar, K.B.; Hamilton, L.C.; Kenchington, E.L.; Scott, D.B. Genetic circumscription of deep-water coral species in Canada using 18S rRNA. In *Cold-Water Corals and Ecosystems*; Springer: Berlin, Germany, 2005; pp. 679–690.

27.　Thompson, J.D.; Higgins, D.G.; Gibson, T.J. CLUSTAL W: Improving the sensitivity of progressive multiple sequence alignment through sequence weighting, position-specific gap penalties and weight matrix choice. *Nucleic Acids Res.* **1994**, *22*, 4673–4680. [CrossRef]

28.　Altschul, S.F.; Gish, W.; Miller, W.; Myers, E.W.; Lipman, D.J. Basic local alignment search tool. *J. Mol. Biol.* **1990**, *215*, 403–410. [CrossRef]

29.　Kimura, M. A simple method for estimating evolutionary rates of base substitutions through comparative studies of nucleotide sequences. *J. Mol. Evol.* **1980**, *16*, 111–120. [CrossRef] [PubMed]

30.　Kumar, S.; Stecher, G.; Tamura, K. MEGA7: Molecular evolutionary genetics analysis version 7.0 for bigger datasets. *Mol. Biol. Evol.* **2016**, *33*, 1870–1874. [CrossRef] [PubMed]

31.　Darriba, D.; Taboada, G.L.; Doallo, R.; Posada, D. jModelTest 2: More models, new heuristics and parallel computing. *Nat. Methods* **2012**, *9*, 772. [CrossRef]

32. Guindon, S.; Gascuel, O. A simple, fast and accurate method to estimate large phylogenies by maximum-likelihood. *Syst. Biol.* **2003**, *52*, 696–704. [CrossRef]

33. Akaike, H. A new look at the statistical model identification. *IEEE Trans. Autom. Control* **1974**, *19*, 716–723. [CrossRef]

34. Yamaoka, K.; Nakagawa, T.; Uno, T. Application of Akaike's information criterion (AIC) in the evaluation of linear pharmacokinetic equations. *J. Pharmacokinet. Biopharm.* **1978**, *6*, 165–175. [CrossRef]

35. Hurvich, C.M.; Tsai, C.-L. Regression and time series model selection in small samples. *Biometrika* **1989**, *76*, 297–307. [CrossRef]

36. Simmons, M.P.; Ochoterena, H. Gaps as characters in sequence-based phylogenetic analyses. *Syst. Biol.* **2000**, *49*, 369–381. [CrossRef]

37. Young, N.D.; Healy, J. GapCoder automates the use of indel characters in phylogenetic analysis. *BMC Bioinform.* **2003**, *4*, 6. [CrossRef]

38. Felsenstein, J. Confidence limits on phylogenies: An approach using the bootstrap. *Evolution* **1985**, *39*, 783–791. [CrossRef] [PubMed]

39. Huelsenbeck, J.; Ronquist, F. MrBayes: Bayesian inference of phylogeny. *Bioinformatics* **2001**, *17*, 754–755. [CrossRef] [PubMed]

40. Ronquist, F.; Huelsenbeck, J.P. MrBayes 3: Bayesian phylogenetic inference under mixed models. *Bioinformatics* **2003**, *19*, 1572–1574. [CrossRef] [PubMed]

41. Ronquist, F.; Teslenko, M.; Van Der Mark, P.; Ayres, D.L.; Darling, A.; Höhna, S.; Larget, B.; Liu, L.; Suchard, M.A.; Huelsenbeck, J.P. MrBayes 3.2: Efficient Bayesian phylogenetic inference and model choice across a large model space. *Syst. Biol.* **2012**, *61*, 539–542. [CrossRef] [PubMed]

42. Leloup, E.; Alberto, I. *Siphonophores Calycophorides (Suite) et Physophorides Provenant des Campagnes du Prince Albert Ier de Monaco*; Imprimerie de Monaco: Monaco, Monaco, 1936.

43. Margulis, R.Y. Distribution of some siphonophore species of the suborder Physophorae in the Atlantic Ocean. *Vestn. Mosk. Univ.* **1969**, *24*, 17–38.

44. Nogueira, C.R.; Oliveira, S.d.R., Jr. Siphonophora from the coast of Brazil (17ºS to 24ºS). *Bol. Inst. Oceanogr.* **1991**, *39*, 61–69. [CrossRef]

45. Pagès, F.; Gili, J.M. Siphonophores (Cnidaria, Hydrozoa) of the Benguela Current (southeastern Atlantic). *Sci. Mar.* **1992**, *56*, 65–112.

46. Kawamura, T. A report on Japanese siphonophores with special references to new and rare species. *J. Shiga Pref. Jr. Coll. Ser.* **1954**, *2*, 99–129.

47. Yu, P.-W. Seasonal dynamics of siphonophores in the waters off southern and northern Taiwan, 2006. Master's Thesis, National Sun Yat-Sen University, Kaohsiung City, Taiwan, 2013; pp. 1–137.

48. Lo, W.-T.; Kang, P.-R.; Hsieh, H.-Y. Siphonophores from a transect off southern Taiwan between Kuroshio Current and South China Sea. *Zool. Stud.* **2012**, *51*, 1354–1366.

49. Carré, D. Etude du développement d'Halistemma rubrum (Vogt 1852) siphonophore physonecte agalmidae. *Cah. De Biol. Mar.* **1971**, *12*, 77–93.

50. Musayeva, E. Distribution of siphonophores in the eastern part of the Indian Ocean. *Trans. Inst. Oceanol.* **1976**, *105*, 171–197.

51. Bouillon, J.; Medel, M.D.; Pagès, F.; Gili, J.M.; Boero, F.; Gravili, C. Fauna of the Mediterranean hydrozoa. *Sci. Mar.* **2004**, *68*, 5–438. [CrossRef]

Figure S1 Molecular phylogenetic tree of family Agalmatidae based on 18S rRNA data using the maximum likelihood method. The tree with the highest log likelihood (-3961.38) is shown. The analysis involved 90 nucleotide sequences. We eliminated all positions containing gaps and missing data. The number next to the branches represents bootstrap values
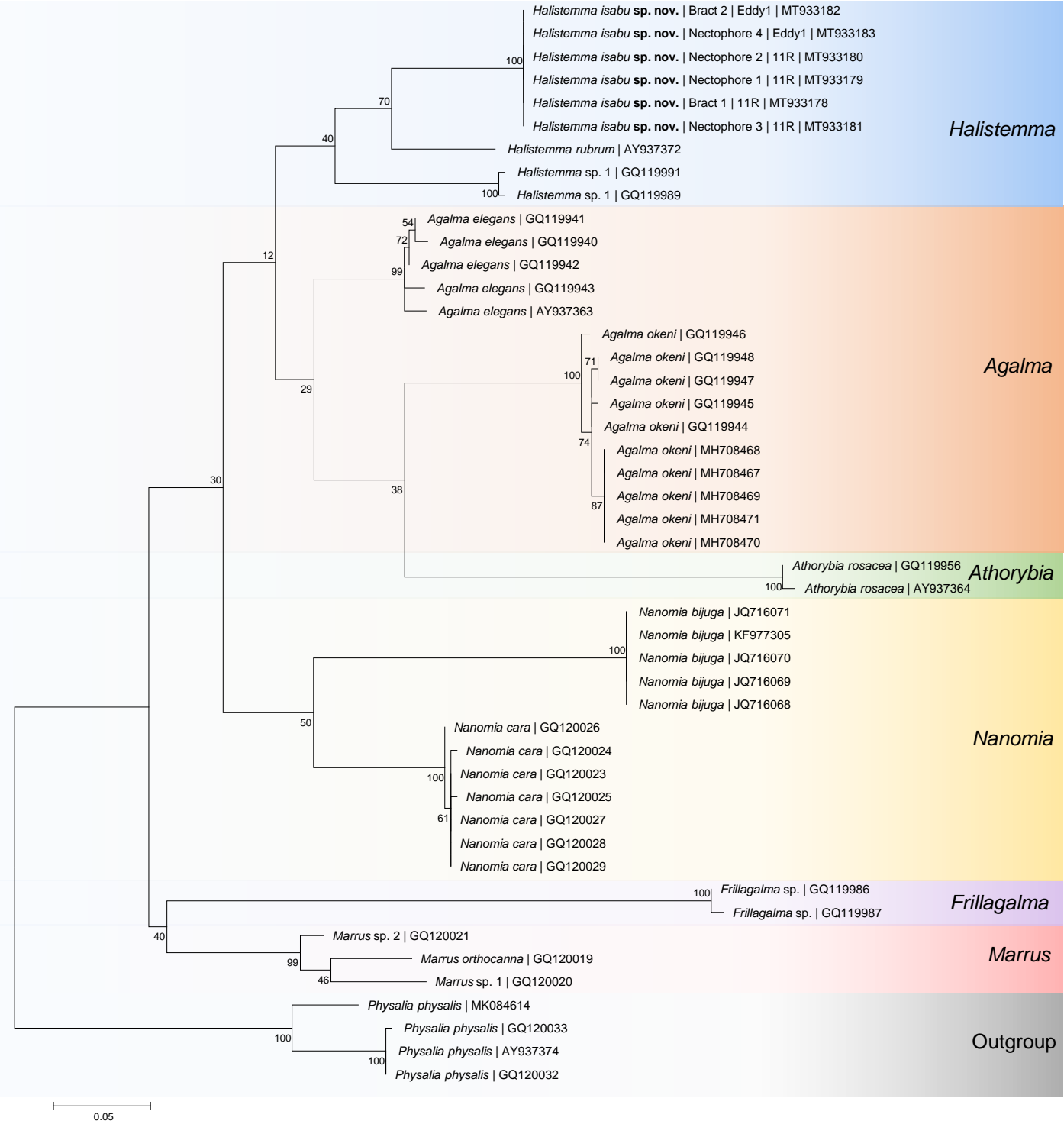
Figure S2 Molecular phylogenetic tree of family Agalmatidae based on mtCOI data using the maximum likelihood method. The tree with the highest log likelihood (-2206.79) is shown. The analysis involved 47 nucleotide sequences. We eliminated all positions containing gaps and missing data. The number next to the branches represents bootstrap values
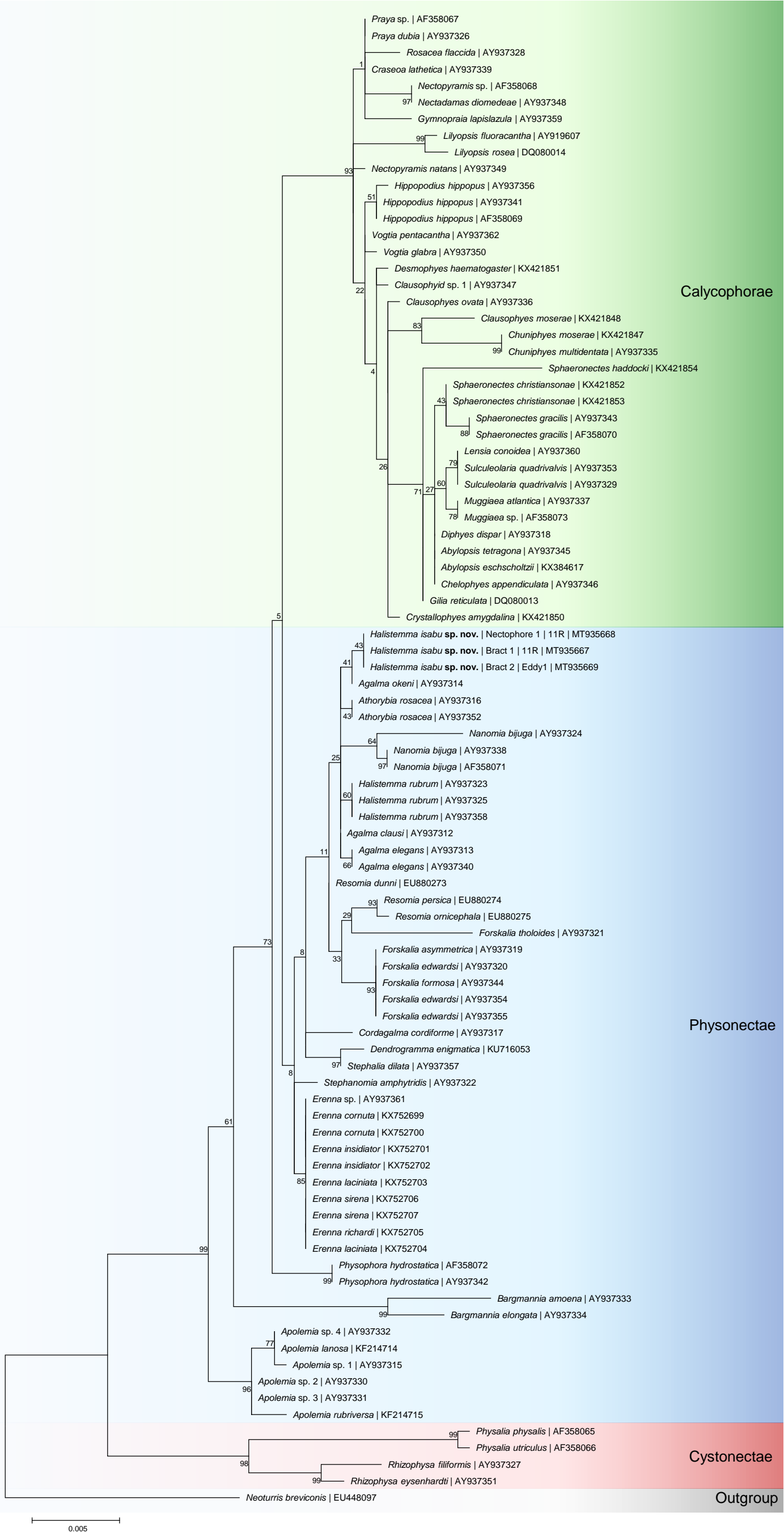
Figure S3 Molecular phylogenetic tree of family Agalmatidae based on 16S rRNA data using the maximum likelihood method. The tree with the highest log likelihood (-1262.61) is shown. The analysis involved 26 nucleotide sequences. We eliminated all positions containing gaps and missing data. The number next to the branches represents bootstrap values.

Table S1 Accession numbers of sequences used in this study's phylogenetic analyses. N: Number of specimens.

Genetic Marker	Model	Suborder	Family	Species	N	Accession Number
Concatenated	GTR+G+I	Physonectae	Agalmatidae	*Halistemma isabu* **sp. nov.**	3	MT933178–MT933179, MT933182, MT935660–MT935661, MT935664, MT935667–MT935669
				Halistemma rubrum	1	AY937372, AY935281, AY937323
				Agalma elegans	2	AY937363, AY935271, AY937313, GQ119943, AY935298, AY937340
				Agalma okeni	1	GQ119944, AY935272, AY937314
				Athorybia rosacea	2	AY937364, AY935274, AY937316, GQ119956, AY935310, AY937352
				Nanomia bijuga	2	JQ716068–JQ716069, AY935282, AY937324, AY935296, AY937338
		Cystonectae	Physaliidae	*Physalia physalis**	1	AY937374, AY935284, AF358065
mtCOI	GTR+G+I	Physonectae	Agalmatidae	*Halistemma isabu* **sp. nov.**	6	MT933178–MT933183
				Halistemma rubrum	1	AY937372
				Halistemma sp. 1	2	GQ119989, GQ119991
				Agalma elegans	5	AY937363, GQ119940–GQ119943
				Agalma okeni	10	GQ119944–GQ119948, MH708467–MH708471
				Athorybia rosacea	2	AY937364, GQ119956
				Frillagalma sp.	2	GQ119986–GQ119987
				Marrus orthocanna	1	GQ120019
				Marrus sp. 1	1	GQ120020
				Marrus sp. 2	1	GQ120021
				Nanomia bijuga	5	JQ716068–JQ716071, KF977305
				Nanomia cara	7	GQ120023–GQ120029
		Cystonectae	Physaliidae	*Physalia physalis**	4	AY937374, GQ120032–GQ120033, MK084614
16S rRNA	T92+G	Physonectae	Agalmatidae	*Halistemma isabu* **sp. nov.**	6	MT935660–MT935665
				Halistemma rubrum	3	AY935281, AY935283, AY935316
				Halistemma sp.	1	KJ816934
				Agalma clausi	1	AY935270
				Agalma elegans	2	AY935271, AY935298
				Agalma okeni	1	AY935272
				Athorybia rosacea	2	AY935274, AY935310
				Lychnagalma urticularia	1	DQ080009
				Marrus claudanielis	1	DQ080007
				Marrus orthocanna	2	DQ080010, KJ866186
				Nanomia bijuga	5	AY935282, AY935296, KF977400–KF977402
		Cystonectae	Physaliidae	*Physalia physalis**	1	AY935284

18S rRNA	K2+G+I	Physonectae	Agalmatidae	*Halistemma isabu* **sp. nov.**	3	MT935667–MT935669
				Halistemma rubrum	3	AY937323, AY937325, AY937358
				Agalma clausi	1	AY937312
				Agalma elegans	2	AY937313, AY937340
				Agalma okeni	1	AY937314
				Athorybia rosacea	2	AY937316, AY937352
				Nanomia bijuga	3	AF358071, AY937324, AY937338
			Apolemiidae	*Apolemia lanosa*	1	KF214714
				Apolemia rubriversa	1	KF214715
				Apolemia sp. 1	1	AY937315
				Apolemia sp. 2	1	AY937330
				Apolemia sp. 3	1	AY937331
				Apolemia sp. 4	1	AY937332
			Cordagalmatidae	*Cordagalma cordiforme*	1	AY937317
			Erennidae	*Erenna cornuta*	2	KX752699–KX752700
				Erenna insidiator	2	KX752701–KX752702
				Erenna laciniata	2	KX752703–KX752704
				Erenna richardi	1	KX752705
				Erenna sirena	2	KX752706–KX752707
				Erenna sp.	1	AY937361
			Forskaliidae	*Forskalia asymmetrica*	1	AY937319
				Forskalia edwardsi	3	AY937320, AY937354–AY937355
				Forskalia formosa	1	AY937344
				Forskalia tholoides	1	AY937321
			Physophoridae	*Physophora hydrostatica*	2	AF358072, AY937342
			Pyrostephidae	*Bargmannia amoena*	1	AY937333
				Bargmannia elongata	1	AY937334
			Resomiidae	*Resomia dunni*	1	EU880273
				Resomia ornicephala	1	EU880275
				Resomia persica	1	EU880274
			Rhodaliidae	*Dendrogramma enigmatica*	1	KU716053
				Stephalia dilata	1	AY937357
			Stephanomiidae	*Stephanomia amphytridis*	1	AY937322
		Calycophorae	Abylidae	*Abylopsis eschscholtzii*	1	KX384617
				Abylopsis tetragona	1	AY937345
			Clausophyidae	*Chuniphyes moserae*	1	KX421847

		Chuniphyes multidentata	1	AY937335
		Clausophyes moserae	1	KX421848
		Clausophyes ovata	1	AY937336
		Clausophyid sp. 1	1	AY937347
		Crystallophyes amygdalina	1	KX421850
	Diphyidae	*Chelophyes appendiculata*	1	AY937346
		Diphyes dispar	1	AY937318
		Gilia reticulata	1	DQ080013
		Lensia conoidea	1	AY937360
		Muggiaea atlantica	1	AY937337
		Muggiaea sp.	1	AF358073
		Sulculeolaria quadrivalvis	2	AY937329, AY937353
	Hippopodiidae	*Hippopodius hippopus*	3	AF358069, AY937341, AY937356
		Vogtia glabra	1	AY937350
		Vogtia pentacantha	1	AY937362
	Prayidae	*Craseoa lathetica*	1	AY937339
		Desmophyes haematogaster	1	KX421851
		Gymnopraia lapislazula	1	AY937359
		Lilyopsis fluoracantha	1	AY919607
		Lilyopsis rosea	1	DQ080014
		Nectadamas diomedeae	1	AY937348
		Nectopyramis natans	1	AY937349
		Nectopyramis sp.	1	AF358068
		Praya dubia	1	AY937326
		Praya sp.	1	AF358067
		Rosacea flaccida	1	AY937328
	Sphaeronectidae	*Sphaeronectes christiansonae*	2	KX421852–KX421853
		Sphaeronectes gracilis	2	AF358070, AY937343
		Sphaeronectes haddocki	1	KX421854
Cystonectae	Physaliidae	*Physalia physalis*	1	AF358065
		Physalia utriculus	1	AF358066
	Rhizophysidae	*Rhizophysa eysenhardti*	1	AY937351
		Rhizophysa filiformis	1	AY937327
Filifera	Pandeidae	*Neoturris breviconis**	1	EU448097

* Outgroup

Table S2 K2P distances of mtCOI sequences between genus *Halistemma* from Genbank and this study. Standard error estimates are shown above the diagonal with italics.

mtCOI	1	2	3	4	5	6	7	8	9
1. *Halistemma rubrum* ǀ AY937372		*0.015*	*0.015*	*0.015*	*0.015*	*0.015*	*0.015*	*0.015*	*0.015*
2. *Halistemma* sp. 1 ǀ GQ119989	0.122		*0.002*	*0.015*	*0.015*	*0.015*	*0.015*	*0.015*	*0.015*
3. *Halistemma* sp. 1 ǀ GQ119991	0.122	0.003		*0.015*	*0.015*	*0.015*	*0.015*	*0.015*	*0.015*
4. *Halistemma isabu* **sp. nov.** ǀ Nectophore 1 ǀ 11R ǀ MT933179	0.120	0.122	0.120		*0.000*	*0.000*	*0.000*	*0.000*	*0.002*
5. *Halistemma isabu* **sp. nov.** ǀ Nectophore 2 ǀ 11R ǀ MT933180	0.120	0.122	0.120	0.000		*0.000*	*0.000*	*0.000*	*0.002*
6. *Halistemma isabu* **sp. nov.** ǀ Nectophore 3 ǀ 11R ǀ MT933181	0.120	0.122	0.120	0.000	0.000		*0.000*	*0.000*	*0.002*
7. *Halistemma isabu* **sp. nov.** ǀ Nectophore 4 ǀ Eddy1 ǀ MT933183	0.120	0.122	0.120	0.000	0.000	0.000		*0.000*	*0.002*
8. *Halistemma isabu* **sp. nov.** ǀ Bract 1 ǀ 11R ǀ MT933178	0.120	0.122	0.120	0.000	0.000	0.000	0.000		*0.002*
9. *Halistemma isabu* **sp. nov.** ǀ Bract 2 ǀ Eddy1 ǀ MT933182	0.118	0.124	0.122	0.002	0.002	0.002	0.002	0.002	

Table S3 K2P distances of 16S rRNA sequences between genus *Halistemma* from Genbank and this study. Standard error estimates are shown above the diagonal with italics.

16S rRNA	1	2	3	4	5	6	7	8	9	10
1. *Halistemma rubrum* | AY935281		*0.000*	*0.011*	*0.031*	*0.026*	*0.026*	*0.026*	*0.026*	*0.026*	*0.027*
2. *Halistemma rubrum* | AY935283	0.000		*0.011*	*0.031*	*0.026*	*0.026*	*0.026*	*0.026*	*0.026*	*0.027*
3. *Halistemma rubrum* | AY935316	0.022	0.022		*0.031*	*0.028*	*0.028*	*0.028*	*0.028*	*0.028*	*0.029*
4. *Halistemma* sp. | KJ816934	0.148	0.148	0.141		*0.029*	*0.029*	*0.029*	*0.029*	*0.029*	*0.030*
5. *Halistemma isabu* **sp. nov.** | Nectophore 1 | 11R | MT935661	0.113	0.113	0.120	0.133		*0.000*	*0.000*	*0.000*	*0.000*	*0.008*
6. *Halistemma isabu* **sp. nov.** | Nectophore 2 | 11R | MT935662	0.113	0.113	0.120	0.133	0.000		*0.000*	*0.000*	*0.000*	*0.008*
7. *Halistemma isabu* **sp. nov.** | Nectophore 3 | 11R | MT935663	0.113	0.113	0.120	0.133	0.000	0.000		*0.000*	*0.000*	*0.008*
8. *Halistemma isabu* **sp. nov.** | Nectophore 4 | Eddy1 | MT935665	0.113	0.113	0.120	0.133	0.000	0.000	0.000		*0.000*	*0.008*
9. *Halistemma isabu* **sp. nov.** | Bract 1 | 11R | MT935660	0.113	0.113	0.120	0.133	0.000	0.000	0.000	0.000		*0.008*
10. *Halistemma isabu* **sp. nov.** | Bract 2 | Eddy1 | MT935664	0.127	0.127	0.134	0.147	0.011	0.011	0.011	0.011	0.011	

Table S4 K2P distances of 18S rRNA sequences between genus *Halistemma* from Genbank and this study. Standard error estimates are shown above the diagonal with italics.

18S rRNA	1	2	3	4	5	6
1. *Halistemma rubrum* | AY937323		*0.000*	*0.000*	*0.001*	*0.001*	*0.001*
2. *Halistemma rubrum* | AY937325	0.000		*0.000*	*0.001*	*0.001*	*0.001*
3. *Halistemma rubrum* | AY937358	0.000	0.000		*0.001*	*0.001*	*0.001*
4. *Halistemma isabu* **sp. nov.** | Nectophore 1 | 11R | MT935668	0.002	0.002	0.002		*0.000*	*0.000*
5. *Halistemma isabu* **sp. nov.** | Bract 1 | 11R | MT935667	0.002	0.002	0.002	0.000		*0.000*
6. *Halistemma isabu* **sp. nov.** | Bract 2 | Eddy1 | MT935669	0.002	0.002	0.002	0.000	0.000	

Table S5 Estimates of average K2P distances over sequence pairs within family Agalmatidae, based on mtCOI, 16S rRNA and 18S rRNA gene data.

Taxonomic group	mtCOI			16S rRNA			18S rRNA		
	N	Min–Max (Average)	Standard deviation	N	Min–Max (Average)	Standard deviation	N	Min–Max (Average)	Standard deviation
Intraspecies	35	0.000–0.022 (0.005)	0.006	16	0.000–0.480 (0.080)	0.152	11	0.000–0.005 (0.001)	0.002
Interspecies	36	0.098–0.212 (0.176)	0.025	19	0.059–0.510 (0.179)	0.100	13	0.001–0.008 (0.003)	0.002
Instragenus	36	0.098–0.172 (0.147)	0.019	14	0.059–0.149 (0.116)	0.019	10	0.001–0.002 (0.002)	0.001
Halistemma	9	0.098–0.131 (0.119)	0.014	10	0.108–0.149 (0.121)	0.013	6	0.002–0.002 (0.002)	0.000
Agalma	15	0.138–0.150 (0.144)	0.004	4	0.059–0.108 (0.088)	0.021	4	0.001–0.001 (0.001)	0.000
Nanomia	12	0.168–0.172 (0.169)	0.002	-	-	-	-	-	-
Intergenus	36	0.134–0.212 (0.183)	0.021	19	0.083–0.510 (0.198)	0.106	13	0.001–0.008 (0.004)	0.002